Available online at www.sciencedirect.com
SCIENCE DIRECT
Journal of Asian Earth Sciences 26 (2006) 585–604
Journal of Asian Earth Sciences
www.elsevier.com/locate/jaes

Palaeoproterozoic metamorphism in the Jeori-Wangtu Gneissic Complex (JWGC), western Himalayas ☆

N.C. Pant[a,*], A. Kundu[a], Rakesh Kumar[a], B.S. Dorka[b], S. Prasher[b,✠]

[a] *EPMA Laboratory, Geological Survey of India, NH-5P, NIT, Faridabad 121001, India*
[b] *Geological Survey of India, Chandigarh, India*

Received 1 December 2002; revised 1 September 2004; accepted 6 December 2004

Abstract

The Jeori-Wangtu Gneissic Complex (JWGC) exposed as a tectonic window in the Lesser Himalayas represents one of the oldest Gneissic Complex of the Himalayas. Foliated granite and the metapelite constitute the dominant lithologies of the JWGC. The western margin of the JWGC is bounded by a brittle shear while in the east, the tectonic surface is a ductile shear zone.

Kyanite schist, chloritoid schist, staurolite schist (St-1), garnet schist and staurolite schist (St-2) are present in a west to east sequence beginning from near to the Jhakhri thrust and up to the contact with the JWGC granite. Mica schist is intermittently present and is the dominant metapelite. Low to medium grade regional metamorphic conditions has been inferred for these rocks.

Calc silicate enclaves within the JWGC granite preserve the contact metamorphic effects. These are reflected in development of narrow zones of disequilibrium assemblages of calcareous garnet ($grs_{\sim 53}$), clinopyroxene, K feldspar, calcic plagioclase (An_{86}), quartz, zoned sphene, zoned allanite, amphiboles, calcite and epidote.

Recording of contact metamorphic assemblage of 1.80 Ga granite witin the enclave calc silicates and in the host metapelites over an earlier, relict low to medium grade assemblage indicates that the JWGC preserves palaeoproterozoic metamorphic imprints.

Keywords: Pre-Himalayan metamorphism; Western Himalayas; Contact metamorphism

1. Introduction

The Himalayas can be considered to be composed of several, linear and generally continuous lithotectonic domains (Gansser, 1964). In a north to south transect these are (a) the Tethyan Himalaya or Tethyan Zone, (b) the Higher/Greater Himalaya or the Central Crystalline Zone, (c) the Lesser Himalaya and (d) the Sub-Himalayan Zone. The Greater and Lesser Himalayas represent Indian continental crust and are separated by the Main Central Thrust along which the former is thrusted over the latter. The Palaeogene foreland basin sedimentary rocks are also present in the Lesser Himalayas. Late Proterozoic to Cambrian rocks of the Greater Himalayas are regionally metamorphosed and intruded by leucogranite melts (Parrish and Hodges, 1996) while Middle Proterozoic to Palaeozoic (Frank et al., 1977; Bhanot et al., 1978; Valdiya, 1980; LeFort et al., 1983; Thakur, 1983; Pognante and Lombardo, 1989; Parrish and Hodges, 1996) Indian continental crust rocks of the Lesser Himalayas are non-metamorphosed to weakly metamorphosed. The age of high temperature metamorphism can be constrained in the region of 20–22 Ma based mainly on U–Th–Pb dates of leucogranites (eg. Searle, 1999). All other metamorphic events can be considered pre-Himalayan. The pre-Himalayan metamorphic rocks find passing mention in many studies (e.g. Pognante and Lombardo, 1989; Verma, 1989; Searle et al., 1992) but no detailed characterization is available. In the Greater as well as the Lesser Himalayas several pre-Himalayan granite intrude the Indian continental crustal and sedimentary rocks. The study of these granites and their

☆ Originally submitted for the 17 Himalaya Tibet Worshop
* Corresponding author. Tel./fax: +91 129 2420763.
E-mail address: pantnc@rediffmail.com (N.C. Pant).
✠ Deceased on 16th September 2002.

1367-9120/$ - see front matter © 2005 Elsevier Ltd. All rights reserved.
doi:10.1016/j.jseaes.2004.12.004

thermal effects on the continental crustal hosts is important for evolving models of pre-collision margins as well as for understanding the basement cover relationships for the younger sedimentary rocks.

In the western Himalayas in northwest India, the Larji-Kullu-Rampur Window (LKRW; Berthelsen, 1951; Jhingaran et al., 1952; Thoni, 1977) in the uppermost part of the Lesser Himalayas contains the Jeori-Wangtu-Gneissic-Complex (JWGC) in its southern part (Bhargava et al., 1972) and is thrusted over the Rampur Group near the town of Jhakhri (Fig. 1). The JWGC is made up of orthogenisses (the Wangtu gneisses herein referred as the JWGC granite) and paragneisses alongwith subordinate metabasites and minor calc silicates. The JWGC granite has been subjected to several geochronological studies (Rb–Sr whole rock ages of 2025 ± 86 Ma, Kwatra et al., 1986; U–Pb zircon age of 1866 ± 10 Ma, Singh et al., 1994; Rb–Sr whole rock ages of 1866 ± 64, Rameshwar et al., 1995; U–Pb zircon age of 1840 ± 16 Ma, Miller et al., 2000) that indicates the granite magmatism to be of the early to mid-Proterozoic age.

In this study a petrological evaluation of paragneisses occurring in association with the Proterozoic acid magmatism in the JWGC has been carried out with an attempt to record the pre-Himalayan regional and thermal metamorphic conditions in the northwest Himalayas.

2. Geological setup

The JWGC is exposed as a tectonic sheet of 60–80 km width in the uppermost part of the Lesser Himalayas of the Himachal Pradesh between 1.5 km west of Jhakhri in the west to close to the confluence of the Sutlej and the Baspa Rivers near Karcham in the east. The JWGC has also been considered as part of the Larji-Kullu-Rampur Window (LKRW; e.g. Miller et al., 2000 and Fig. 1) with the thrust close to Jhakhri separating it from rest of the LKRW components. The JWGC represents the oldest rock units in the LKRW. Towards its western margin it overlies the Rampur Group rocks (quartzite and metavolcanics) and the contact is marked by an east-dipping fault (at Barauni Nala) and is characterized by brittle deformation in the underlying rocks. The eastern margin of the JWGC tectonic sheet is marked by an easterly dipping ductile shear as evidenced by the presence of thin, boudinaged quartzo-feldspathic veins, recrystallized calc silicates and remobilised Fe–Cu sulphides. The JWGC is overlain by a quartzite followed by calc silicates-metapelite sequence (Jutogh Group?). Sharma and Misra (1998) have invoked the presence of the Chail Thrust between Jhakhri and Jeori and described the ductile shear at Karcham as the Jutogh Thrust, thus, dividing the JWGC package into Chail and Jutogh rocks (Figs. 1 and 2 of Sharma and Mishra, op cit.) which is erroneous as the sequence described as the Jutogh Group is mainly foliated granite of the JWGC. The base of the JWGC is not exposed.

About 70% of the exposed rocks within the JWGC are foliated granite while the rest are metapelites with subordinate amphibolites and calc silicates. The metapelites occur in the western part while the central and the eastern areas expose the granite.

Calc silicates occur in two distinct zones namely, the Taranda Zone and the Karcham Zone. The former is well inside the JWGC and occurs as enclave within granite while the latter lies east of eastern ductile sheared margin of JWGC.

Taranda Zone. This zone is located within the JWGC granite west of the Soldan Nala. The composite thickness of the Taranda calc silicate zone is ~35 m. The traverse log of the zone is given in Fig. 2. The first calc silicate zone (Zone A; Fig. 2) is ~20 m thick. It is bound on the east and the west by thin aplite bands. Within these two aplitic bands the calc silicate beds are few centimetres to 3–4 m thick and are interspersed with biotite granite. The western aplitic band is in contact with the porphyritic granite (two feldspar biotite granite) on one side. In the second zone (Zone B; Fig. 2), calc silicate occurs interbanded with tourmaline bearing pegmatite/granite. Amphibolite is also present in this zone. In the third sub-zone of the Taranda Zone (Zone C; Fig. 2), the calc silicate proportion is highest. This zone is around 13 m thick. Calc silicate in Zone C is bound in on one side by the porphyritic granite and towards other by the tourmaline pegmatite.

3. Petrography

The foliated granite and the metapelites constitute the dominant lithology of the JWGC. The calc silicates occur as enclave within the granite. The amphibolite is mainly present within the metapelite.

3.1. Metapelites

The main component of the metapelite is the mica schist (biotite–muscovite ± chlorite schist; phyllosilicates > 50%) with several interspersed amphibolite/amphibole schist (Fig. 1). In the mica schist the proportion of muscovite, biotite and chlorite is highly variable. Quartz is the dominant leucocratic mineral though locally, sodic plagioclase is also present, especially close to the granite apophyses which sporadically occur in this low-grade schist. The metapelites have a well-developed foliation defined mainly by muscovite and biotite (except in St-2 in which biotite is the dominant mica). Within the mica schist kyanite, chloritoid, staurolite (St-1), garnet and staurolite (St-2) schists occur progressively from western margin of the metapelite exposure to its contact with the JWGC granite. These schists are distinguishable on the basis of distinct assemblages (Table 1).

The Kyanite schist is highly friable, locally kinked and puckered. In thin sections nearly 50% of the rock is made up of phyllosilicates dominated by muscovite. Muscovite is

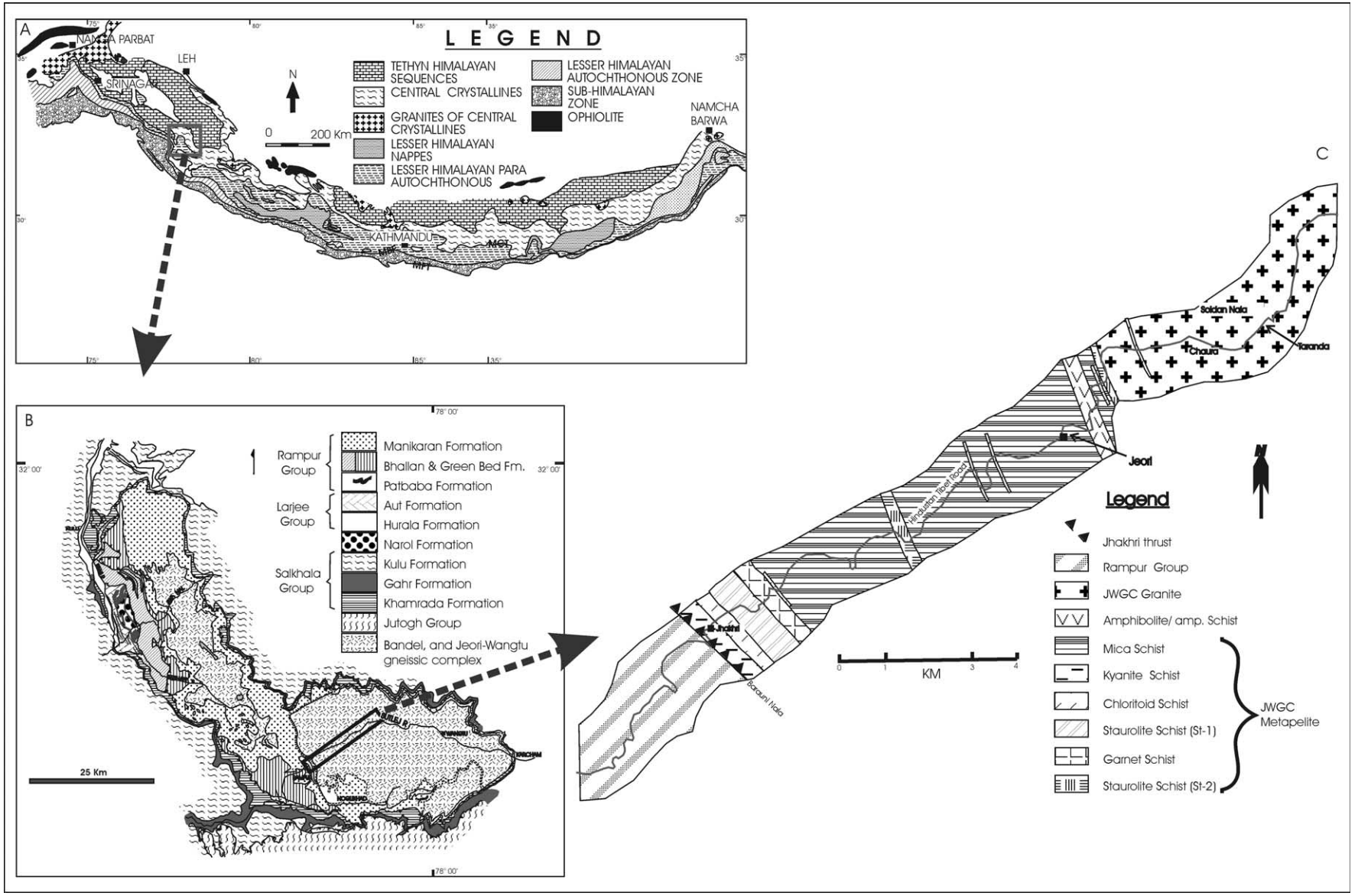

Fig. 1. A traverse map of the western part of the JWGC in regional context, (A) Simplified geological map of the Himalayas (Modified after Gansser, 1964) showing location of the JWGC, (B) Geological map of the Larji-Kullu-Rampur Window (LKRW) with the area of interest demarcated (map from Bhargava, 1982), (C) Traverse geological map along a part of the Hindustan-Tibet Road (NH-22) covering Jhakhri to Taranda within the JWGC.

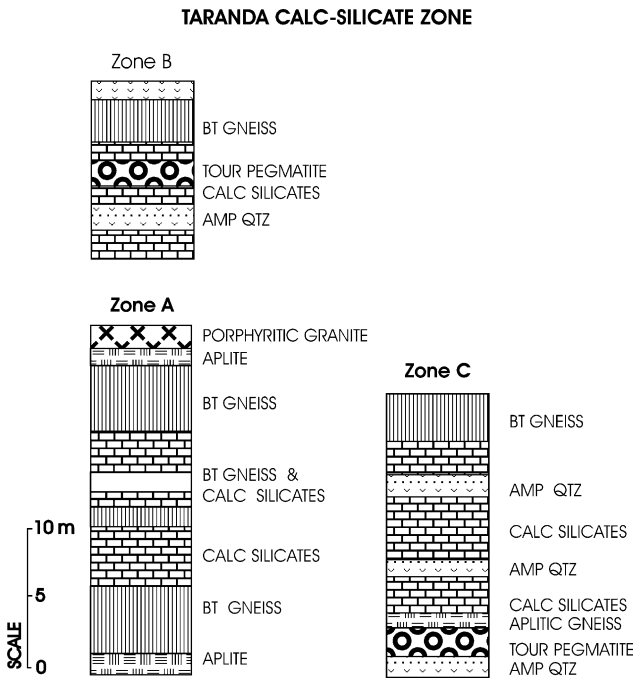

Fig. 2. Lithologs of calc silicates of the Taranda Calc Silicate Zone. (Bt-Biotite; Amp-Amphibole; Tour-Tormaline; Qtz-Quartzite).

inequigranular (0.01–>1 mm) and is locally porphyroblastic. Quartz is anhedral and inequigranular. Chlorite is subordinate and subhedral. Kyanite occurs as stout, subhedral grains in the matrix. Zircon is a common accessory. Ilmenite and magnetite coexist in the kyanite schist. The representative assemblage of the kyanite schist is listed in Table 1.

The Chloritoid schist contains colourless to blue, pleochroic, prismatic and locally poikiloblastic (Fig. 3a) porphyroblasts (0.1–>1 mm) of chloritoid which occur parallel as well as across the major foliation. Quartz and muscovite form the dominant matrix minerals. Kyanite coexists with chloritoid (Fig. 3b). Ilmenite and rutile are also observed (Table 1).

The Staurolite schist (St-1) contains staurolite coexisting with chloritoid in absence of kyanite (Table 1). Staurolite is subhedral (Fig. 3c) fine grained (0.1–0.7 mm), sieve textured as well as inclusion free and moderately pleochroic from yellow to golden yellow. Staurolite porphyroblasts occur parallel as well as across to the foliation. Quartz and muscovite are the other significant constituents. Minor chlorite is always associated with staurolite. Ilmenite is commonly present opaque and it occasionally mantles rutile.

The Garnet schist contains xenoblastic to subidioblastic, poikiloblastic and medium to coarse-grained garnets, fine-grained (0.03–0.5 mm) plagioclase (~15%) besides biotite and quartz (Table 1). Epidote and chlorite are present as minor constituents. Inclusion of quartz, ilmenite, muscovite and plagioclase are observed within garnet. Garnet is syn to post-tectonic as evidenced by inclusion trails of ilmenite that continue through it (Fig. 3d). Though mostly of nearly circular cross section, garnets are occasionally elongated in appearance. Growth of the garnet follows matrix plagioclase (Fig. 3e). This is corroborated by the development of patchy zoning in matrix plagioclase due to selective incorporation of Ca from plagioclase in the garnet. In this process the matrix quartz gets enclosed resulting in 'sieve' textured post-tectonic garnet commonly at the margins of large garnet pophyroblasts.

The Staurolite schist (St-2) is separated from St-1 by the garnet schist. The mineralogy of St-2 is different from St-1 (Table 1) in absence of chloritoid, biotite being the dominant phyllosilicate rather than muscovite and presence of plagioclase (Fig. 3f). Staurolite is fine grained and generally inclusion free. Monazite grains are widespread in St-2.

3.2. Calc silicate enclave within the JWGC granite

The calc silicates in Zone A contains calcite, calcic plagioclase, K feldspar, biotite, clinopyroxene, amphibole, quartz (rare), zoned sphene, zoned allanite and zircon (Table 1). The rock is fine grained (0.2–0.7 mm) and generally equigranular. Zircon is fine grained (~0.02 mm) and subhedral. There are distinct amphibole-clinopyroxene rich and biotite rich zones of millimetre scale thickness with biotite very low or nearly absent in the amphibole rich zones and vice versa. The arrangements of these bands define an S-surface, which is parallel to the contact of the calc silicates with the granite. Calcite with rare

Table 1
List of mineral assemblages in the JWGC metapelites

	Assemblage
Schist unit	
Kyanite Schist	Muscovite–kyanite–quartz–ilmenite–magnetite–zircon
Chloritoid Schist	Chloritoid–kyanite–muscovite–quartz–ilmenite–rutile
Staurolite Schist (St-1)	Staurolite–chloritoid–muscovite–quartz–ilmenite ± chlorite
Garnet Schist	Garnet–biotite–plagioclase–muscovite–quartz–ilmenite + chlorite ± epidote
Staurolite Schist (St-2)	Staurolite–biotite–plagioclase–quartz–ilmenite ± sphene ± chlorite
Calc silicate unit	
Zone A	Calcite–plagioclase–K feldspar–biotite–hedenbergite–ferro tschermakite–sphene–zircon ± quartz
Zone B	Calcite–hedenbergite–garnet–quartz ± epidote
Zone C	Calcite–plagioclase–hedenbergite–garnet–apatite–sphene ± scapolite

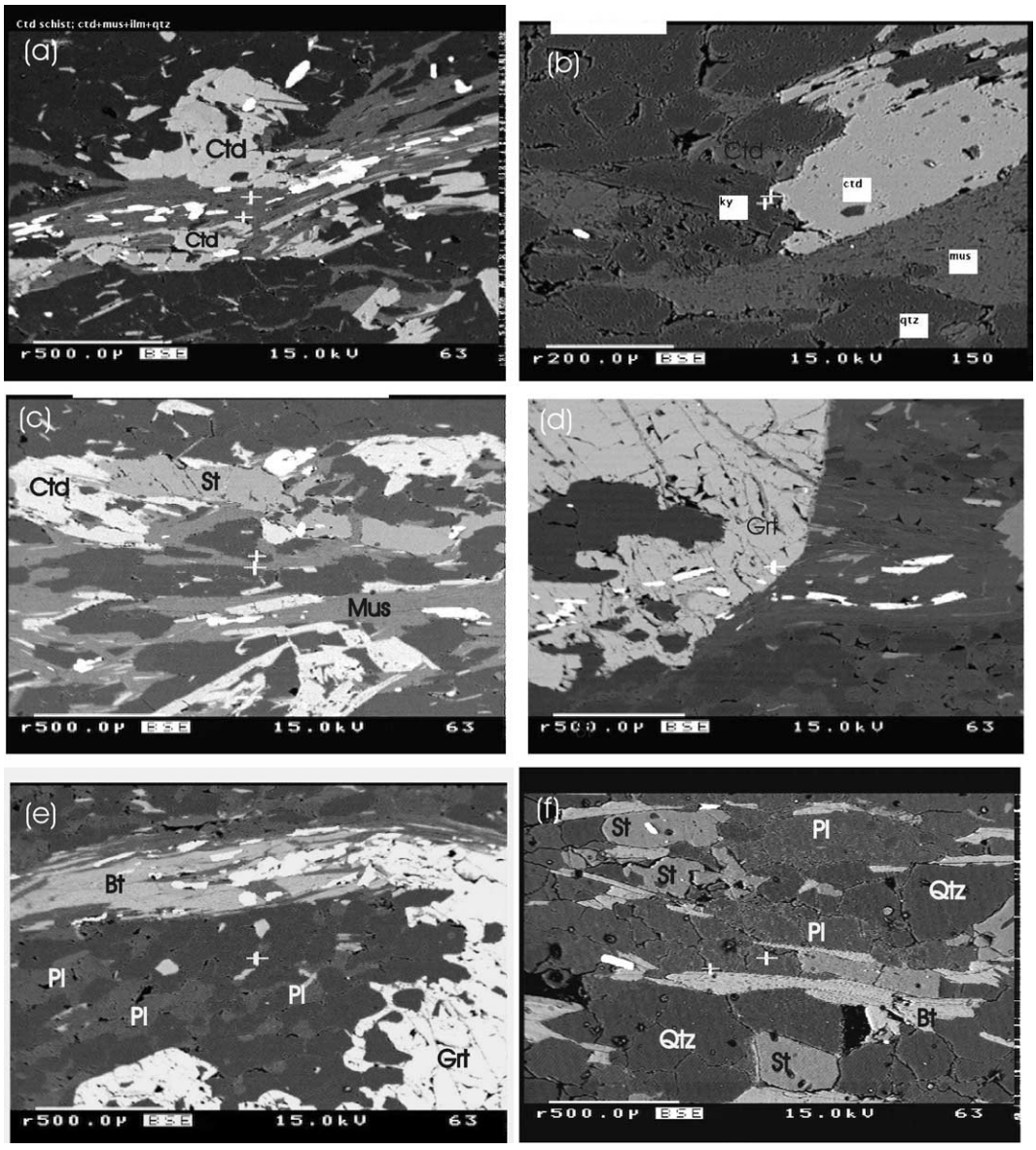

Fig. 3. Back scattered electron (BSE) images of JWGC metapelites (a) Chloritoid schist showing a large and several smaller chloritoid (Ctd) porphyroblasts in quartz (dark) and muscovite (intermediate grey tone) matrix. Bright mineral is ilmenite. (b) Chloritoid schist in which chloritoid (ctd) porphyroblast occurs with kyanite (ky). (c) Staurolite schist (St-1) in which coexisting staurolite and chloritoid are nearly parallel to the foliation. (d) Garnet schist-Note poikiloblastic nature of garnet (Grt) at the margins. Also seen is the continuation of internal inclusion trail (Si) defined by ilmenite as external foliation (Se). Inclusions of quartz, plagioclase, muscovite and ilmenite are common. (e) Garnet schist showing garnet growth following matrix plagioclase leading to the poikiloblastic texture in rim part. Quartz has the darkest tone while plagioclase is slightly lighter toned. (f) Staurolite schist (St-2) which has biotite as the main mica and significant amount of plagioclase in the matrix in contrast to St-1.

quartz inclusion shows development of zoned allanite at its margins (Fig. 4a). Allanite is fine grained (0.005–0.04 mm) and subhedral. Sphene with some Al-zoning (rims richer in Al_2O_3 by ~2 wt %) is present in vicinity of this calcite. Coexisting clinopyroxenes and amphiboles are also present in the calc silicates of Zone A. In Zone B clinopyroxene (up to 4.5 mm), garnet, quartz, epidote, pyrite, chalcopyrite are present in decreasing order of abundance with clinopyroxene forming the dominant constituent in this inequigranular rock (Fig. 4b). Garnet, anhedral and fine grained generally occurs close to the margins of clinopyroxene. Calcite forms part of the assemblage (Table 1). Clinopyroxene is occasionally enclosed within the sulphides. In localized domains the texture is granoblastic but the mineral proportions vary across the thin sections (e.g. garnet rich, clinopyroxene rich or epidote rich zones). As is evident from above all the compositions are iron-rich. In this zone of the Taranda calc silicate, fair amount (~5%) of sulfides (Fe/Fe–Cu) are recorded. Feldspars are noticeably absent in Zone B. In the Zone C plagioclase, clinopyroxene, garnet, epidote, scapolite, calcite, quartz, apatite, sphene and zircon are

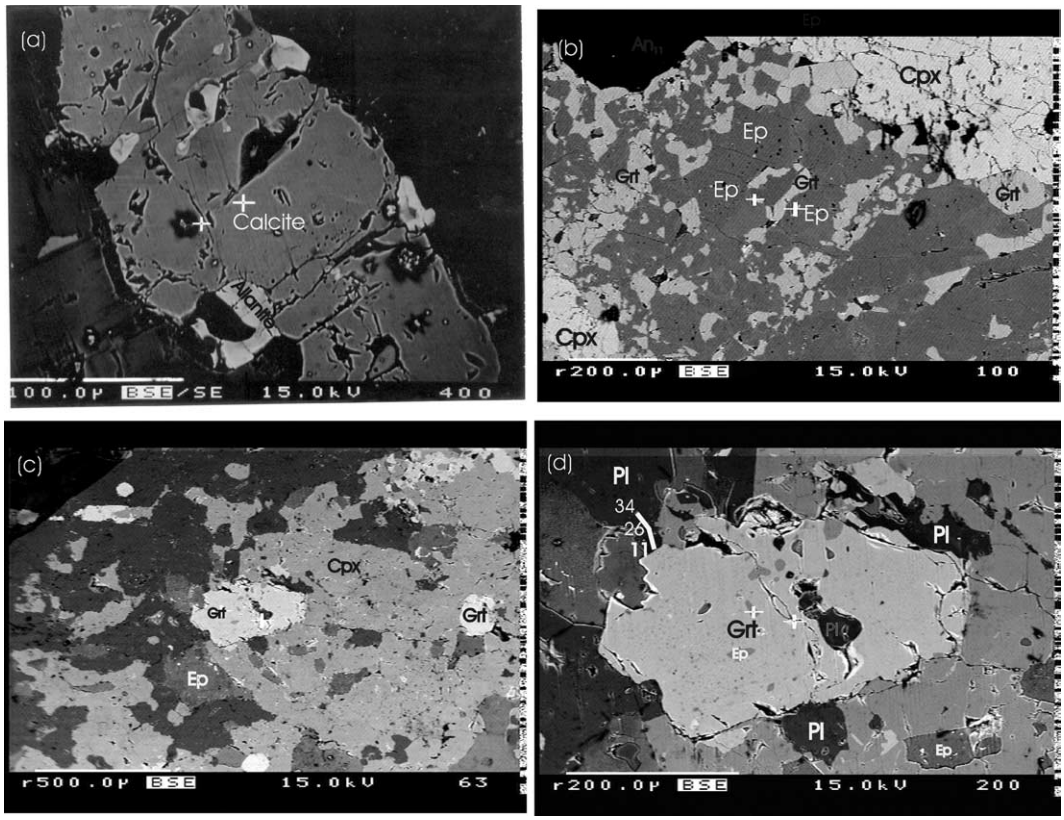

Fig. 4. BSE image of calc silicates of the Taranda Zone (a) Zone A-showing development of zoned allanite at the margins of calcite. Sphene is present in the vicinity. (b) Zone B-this calc silicate has presence of coarse clinopyroxene (Cpx) in the north-eastern and south-western corners with garnet adjacent to the clinopyroxene. The central zone is made up of fine grained coronal garnets around epidote (Ep). (c) Zone C-Note presence of garnet (Grt) in this zone partially within aggregate of clinopyroxene. Other minerals present include Epidote (Ep) and plagioclase (Pl). (d) Zone C-Enlarged BSE image of garnet of Fig. 4(c). It shows presence of epidote (Ep) and plagioclase (Pl) inclusions in garnet. The anorthite content of the plagioclse close to the garnet is given numerically in top left corner. Note the steep zoning profile in plagioclase (from An_{11} in rim adjacent to garnet to An_{34} at a distance of 40 μm inside plagioclase).

present in variable proportions (Table 1). The rock is fine grained (0.2–0.8 mm) and equigranular with nearly equal distribution of felsic and mafic phases. There is domainal concentration of pyroxene/epidote and plagioclase. Both felsic and mafic mineral phases are commonly subhedral. Calcite and quartz, though present, are minor constituents. Rarely scapolite is also present within calcite. Garnet is rare (Fig. 4c) and has inclusions of plagioclase and epidote (Fig. 4d).

3.3. Granite

In the JWGC, granites containing one feldspar one mica, one feldspar two mica, two feldspar one mica, two feldspar two mica and rather rare amphibole granite are present (Pant et al., 2000). The most dominant variants are one feldspar one mica and two feldspar one mica types. The mica in these is almost always biotite. Geochemical signatures of the granite indicate their formation from older continental crust and depleted mantle ages imply contribution from the Archean crust (Miller et al., 2000).

4. Mineral chemistry

Mineral analyses were carried out at EPMA Laboratory, Geological Survey of India, Faridabad on CAMECA SX51 electron microprobe. The operating conditions were 15 kV high voltage and 12 nA current. All analyses were carried out with beam diameter at 1 μm. Natural mineral standards were used for calibration except for Mn and Ti for which a synthetic oxide was used. Automatic PAP correction provided by CAMECA was applied to the raw data.

4.1. Metapelite

Garnet compositions of the JWGC metapelites are listed in Table 2. In general the garnets are Fe rich with almandine component varying between 66 and 80%. The garnet in the garnet schist adjacent to the staurolite schist (St-1) (K-13 and K-89) is more iron rich ($alma_{70–80}$) than the garnet ($alma_{66–70}$) of the garnet schist (K-81) closer to the second stauorlite schist (St-2). There is minor variation in the calcium content of the elongated (inclusion filled) and round (relatively inclusion free) garnets of K-81 with

Table 2
Garnet composition of the JWGC metapelites

No.	Round Garnets		Elongated Garnets					
	[K-81	K-81]	[K-81	K-81]	[K-13	K-13]	[K-89	K-89]
	1	2	3	4	5	6	7	8
	Core	Rim	Core	Rim	Core	Rim	Core	Rim
SiO_2	36.54	36.16	37.20	36.76	36.80	36.75	37.13	37.02
Al_2O_3	20.89	20.25	20.67	20.49	20.97	21.06	20.89	20.83
TiO_2	0.09	0.03	0.06	0.00	0.04	0.00	0.00	0.03
FeO	31.09	31.91	30.47	31.53	32.01	36.71	34.07	34.64
MnO	3.07	2.69	3.38	3.45	3.54	1.84	0.43	0.48
MgO	1.63	1.51	1.82	1.68	1.91	2.30	2.32	2.21
CaO	6.45	5.89	6.50	5.34	4.17	2.13	5.13	4.40
Na_2O	0.01	0.00	0.01	0.01	0.05	0.05	0.00	0.00
K_2O	0.02	0.00	0.01	0.00	0.00	0.00	0.00	0.03
Cr_2O_3	0.17	0.00	0.00	0.01			0.08	0.03
BaO	0.01	0.11	0.00	0.03	0.00	0.00	0.00	0.02
Total	99.97	98.55	100.12	99.30	99.49	100.84	100.05	99.69
	Cation per 12 Oxygen							
Si	2.944	2.965	2.987	2.987	2.985	2.954	2.982	2.991
Aliv	0.056	0.035	0.013	0.013	0.015	0.046	0.018	0.009
Alvi	1.927	1.921	1.943	1.950	1.991	1.948	1.959	1.975
Cr	0.011	0.000	0.000	0.001	0.000	0.000	0.005	0.002
Fe^{+3}	0.108	0.110	0.062	0.062	0.020	0.098	0.050	0.028
Ti	0.005	0.002	0.004	0.000	0.002	0.000	0.000	0.002
Mg	0.196	0.185	0.218	0.204	0.231	0.276	0.278	0.266
Fe^{+2}	1.987	2.077	1.984	2.081	2.152	2.369	2.234	2.313
Mn	0.210	0.187	0.230	0.238	0.243	0.125	0.029	0.033
Ca	0.557	0.517	0.559	0.465	0.362	0.183	0.441	0.381
Total	8.001	7.999	8.000	8.001	8.001	7.999	7.996	8.000
ANDR	0.057	0.057	0.033	0.031	0.011	0.500	0.280	0.015
GROS	0.131	0.118	0.154	0.124	0.110	0.012	0.120	0.112
SPES	0.071	0.063	0.077	0.080	0.081	0.042	0.010	0.011
PYRO	0.066	0.062	0.073	0.068	0.077	0.093	0.093	0.089
ALMA	0.671	0.700	0.663	0.697	0.720	0.802	0.748	0.772
Mg/(Mg+Fe)	0.086	0.078	0.096	0.087	0.096	0.101	0.109	0.102

the elongated garnet being richer in calcium. There is significant zoning of manganese in the garnet of the schist adjacent to staurolite schist (St-1) with core (spss $_8$) having twice the spessertine (spss $_4$) molecule than the rim (K-13).

Biotite has been analysed from the garnet schist, the staurolite schist and the mica schist (Table 3). There is a significant variation of biotite composition within the schists. The most iron rich biotite is of garnet schist (K-13 and K-81) while most magnesian biotite is from staurolite schist (K-21 and K-85; both St-2). The alumina content of the biotite of the mica schist (K-75A and K-88) is lower than that of the biotite of garnet schist and staurolite schist.

Plagioclase compositions from two samples of the mica schist, three samples of the garnet schist and two samples of the staurolite schist are given in Table 4. In the mica schist plagioclase is generally oligoclase ($An_{16–30}$) with occasional presence of albite ($An_{\sim 4}$). In the staurolite schist (K-21 and K-85) of St-2 zone (there is no plagioclase in St-1) andesine plagioclase is present ($An_{<20}$). In the garnet schist (e.g. K-81), the rim plagioclase is slightly more sodic than the core. The included plagioclase (K-81) is distinctly more calcic (by ~13 mole %) than the matrix plagioclase. Rarely symplectitic plagioclase (~An_{87}) indicating decompression is present in the garnet schist while matrix plagioclase is less calcic (~An_{55}).

Staurolite, chloritoid and kyanite analyses are listed in Table 5. Staurolite analyses are from both St-1 (K-11) and St-2 (K-21). Staurolite of St-1, which is associated with chloritoid, is distinctly more zincian (ZnO ~ 2.5%) than that of the St-2 (ZnO ~ 0.56%). The St-2 staurolite also has higher Fe content (FeO ~ 14% vs. 11% of St-1). Staurolite and chloritoid do not show any significant zoning.

Chlorite and epidote analyses are listed in Table 6. Chlorite has been analysed from the mica schist (K-88), the staurolite schist (St-1; K-11), the garnet schist close to granite contact (K-81) and the garnet schist (K-85) close to St-1. The most magnesian chlorite is that of the mica schist. Chlorite of the staurolite schist (St-1) and the garnet schist close to the margin of the JWGC granite is significantly iron-rich (~6–8% higher FeO than the mica schist). In both of these rocks chlorite is modally very low (~2–3%) and bulk of the magnesium of the rock is partitioned in the biotite. It is also of significance to note that the muscovite content of these two schists is relatively low in comparison

Table 3
Biotite composition of the JWGC metapelites

	K-75A	K-81	K-85	K-88	K-13	K-21	K-89
	1	2	3	4	5	6	7
SiO_2	36.74	35.08	36.38	36.88	34.68	35.18	35.43
Al_2O_3	16.32	18.23	18.36	17.84	18.30	19.07	19.02
TiO_2	2.05	2.42	1.25	1.59	1.64	1.69	1.45
FeO	20.75	21.48	17.34	16.21	22.67	19.44	19.16
MnO	0.43	0.10	0.05	0.11	0.09	0.01	0.00
MgO	9.70	7.71	11.06	12.50	8.80	9.32	9.77
CaO	0.00	0.00	0.01	0.00	0.01	0.00	0.02
Na_2O	0.15	0.20	0.26	0.27	0.08	0.37	0.30
K_2O	9.74	9.29	9.58	9.58	8.60	9.41	9.32
Cr_2O_3	0.11	0.05	0.00	0.00	0.00	0.00	0.00
BaO	0.09	0.00	0.00	0.00	0.18	0.30	0.00
Total	96.08	94.56	94.29	94.98	95.05	94.79	94.47
	Cations per 24 O						
Si	5.612	5.445	5.539	5.544	5.369	5.402	5.431
Aliv	2.388	2.555	2.461	2.456	2.631	2.598	2.569
Alvi	0.549	0.781	0.834	0.704	0.709	0.855	0.867
Cr	0.004	0.002	0.000	0.000	0.000	0.000	0.000
Ti	0.236	0.283	0.143	0.180	0.191	0.195	0.167
Fe^{+2}	2.651	2.789	2.208	2.038	2.935	2.497	2.457
Mn	0.055	0.013	0.007	0.015	0.011	0.001	0.000
Mg	2.210	1.785	2.509	2.801	2.055	2.133	2.233
Ca	0.000	0.000	0.001	0.000	0.002	0.000	0.004
Ba	0.005	0.000	0.000	0.000	0.011	0.018	0.000
Na	0.046	0.060	0.076	0.078	0.023	0.110	0.088
K	1.898	1.840	1.860	1.837	1.698	1.844	1.823
OH	4.000	4.000	4.000	4.000	4.000	4.000	4.000
Total	19.654	19.553	19.638	19.653	19.635	19.653	19.639

to the other schist units. Epidote is observed rather sparsely within the garnet schist. There is no significant variation in epidote composition and it is mainly clinozoisite.

4.2. Calc silicates enclave within the JWGC granite

Mineral compositions of the calc silicates are given in Tables 7–10. Amphibole (Table 7) is ferro tschermakite (classification based on Leake et al., 1997). Plagioclase in the Zone A is calcic (An_{86}). Plagioclase of two compositions (Table 8) are present in the Zone C i.e. andesine–labradorite ($An_{\sim 39-42}$) and oligoclase ($An_{\sim 11-13}$). K feldspar ($Or > 98$) is also present though sparingly. Epidote contains significant iron (Table 9) and the grain rims are slightly higher in Fe in comparison to the core. Epidote composition of zone C (Table 9) is quite similar to that of the Zone B. Fe-rich (Mg nearly absent) chlorite has been analysed in zone A. Biotite has nearly equal cationic proportion of Fe^{+2} and Mg (Table 10). Garnet is dominantly grossular ($gros_{53}$) and has significant almandine ($alam_{18-20}$) and andradite ($andr_{\sim 24}$) components (Table 7). Clinopyroxene is Fe rich ($wo > 50$ $en \sim 10$ $fs < 40$) with very low magnesium content ($MgO \sim 3$ wt %) in all the zones. Garnet and clinopyroxene are nearly unzoned. Apatite is almost pure calcium phosphate but in sphene significant aluminium is present ($Al_2O_3 \sim 6$ wt %).

5. Geothermobarometry

The lithologies concerned with the present work are chiefly—the metapelites, the granite (magma temperature) and the calc silicate. The Ti content of biotite has been shown to be temperature dependent (Lal, 1991). Since, biotite is nearly ubiquitously present in all the metapelites, this formulation has been applied. The JWGC granite is intrusive into the metapelite. In context of the contact effect of the granite and its contribution to the reported tin-tungsten mineralization, it is of importance to have an idea of the magma temperature. For this, the apatite and zircon saturation techniques using the bulk chemistry have been applied. The garnet-clinopyroxene exchange geothermometer has been used to estimate the temperature of formation of thermal metamorphic assemblage in the calc silicate.

5.1. Metapelites

In Table 11 temperatures estimated using garnet-biotite Fe–Mg exchange and Ti content of biotite are listed. For garnet-biotite pair's formulations of Ferry and Spear (1978), Dasgupta et al. (1991), Bhattacharya et al. (1992) have been used for temperature estimation. Considering the low to medium grade assemblages, the temperatures have been computed for 4 and 6 kbar pressures. For each of the three

Table 4
Plagioclase composition of the JWGC metapelites

	K-13	K-75A	K-75A	K-81	K-81	K-81	K-85	K-85	K-88	K-88	K-89	K-89	K-21
	1	2	3	4	5	6	7	8	9	10	11	12	13
		Core	Rim	Inc. in gr	Rim adj. gr	Core adj. gr	Coarse	Fine	Core	Rim			
SiO_2	60.66	60.50	61.75	55.99	57.92	57.65	63.67	62.85	63.98	67.37	54.09	45.94	64.54
Al_2O_3	23.95	24.30	24.12	27.58	26.27	25.92	21.71	22.73	21.50	19.83	28.76	32.93	21.83
TiO_2	0.00	0.00	0.00	0.02	0.00	0.00	0.03	0.00	0.00	0.03	0.03	0.00	0.00
FeO	0.22	0.14	0.07	0.74	0.27	0.01	0.01	0.00	0.00	0.17	0.06	0.00	0.09
MnO	0.00	0.00	0.00	0.13	0.00	0.00	0.05	0.06	0.00	0.13	0.04	0.00	0.00
MgO	0.01	0.00	0.00	0.00	0.00	0.00	0.00	0.00	0.00	0.00	0.00	0.00	0.00
CaO	5.34	6.17	5.77	9.79	8.31	8.43	3.60	3.95	3.47	1.00	11.70	17.81	2.95
Na_2O	8.79	7.77	8.54	4.79	7.04	6.73	9.21	9.08	9.74	11.40	5.07	1.51	10.23
K_2O	0.11	0.21	0.25	0.07	0.04	0.11	0.10	0.10	0.12	0.07	0.04	0.00	0.09
P_2O_5	0.09	0.09	0.10	0.00	0.00	0.05	0.00	0.00	0.00	0.00	0.00	0.00	0.07
Cr_2O_3	0.00	0.00	0.08	0.20	0.00	0.02	0.11	0.06	0.03	0.00	0.09	0.04	0.05
BaO	0.00	0.00	0.09	0.01	0.01	0.06	0.00	0.02	0.00	0.00	0.00	0.02	0.00
Total	99.17	99.18	100.77	99.32	99.86	98.98	98.49	98.85	98.84	100.00	99.88	98.25	99.85
	Cations per 8 O												
Si	2.722	2.713	2.731	2.532	2.598	2.609	2.857	2.809	2.856	2.958	2.450	2.154	2.854
Al	1.267	1.284	1.257	1.470	1.389	1.382	1.139	1.197	1.131	1.026	1.535	1.819	1.138
Fe	0.008	0.005	0.003	0.028	0.010	0.000	0.003	0.000	0.000	0.006	0.002	0.000	0.000
Ti	0.000	0.000	0.000	0.001	0.000	0.000	0.001	0.000	0.000	0.001	0.001	0.000	0.000
Mg	0.001	0.000	0.000	0.000	0.000	0.000	0.000	0.000	0.000	0.000	0.000	0.000	0.000
Na	0.765	0.675	0.732	0.420	0.612	0.590	0.794	0.787	0.843	0.970	0.445	0.137	0.880
Ca	0.257	0.296	0.274	0.474	0.399	0.409	0.172	0.189	0.166	0.047	0.568	0.895	0.140
K	0.006	0.012	0.014	0.004	0.002	0.006	0.006	0.005	0.007	0.004	0.002	0.000	0.005
Ba	0.000	0.000	0.002	0.000	0.000	0.001	0.000	0.000	0.000	0.000	0.000	0.000	0.000
Rb	0.000	0.000	0.000	0.000	0.000	0.000	0.000	0.000	0.000	0.000	0.000	0.000	0.000
Cs	0.000	0.000	0.000	0.000	0.000	0.000	0.000	0.000	0.000	0.000	0.000	0.000	0.000
Sr	0.000	0.000	0.000	0.000	0.000	0.000	0.000	0.000	0.000	0.000	0.000	0.000	0.000
Total	5.026	4.986	5.012	4.930	5.010	4.998	4.971	4.988	5.003	5.012	5.004	5.005	5.017
CN	0.000	0.000	0.002	0.000	0.000	0.001	0.000	0.000	0.000	0.000	0.000	0.000	0.000
OR	0.006	0.012	0.014	0.005	0.002	0.006	0.006	0.006	0.007	0.004	0.002	0.000	0.005
AB	0.744	0.686	0.717	0.467	0.604	0.586	0.817	0.801	0.830	0.950	0.439	0.133	0.859
AN	0.250	0.301	0.268	0.528	0.394	0.406	0.177	0.193	0.163	0.046	0.559	0.867	0.137

Inc., inclusion; gr, garnet; adj., adjacent.

Table 5
Kyanite, chloritoid and staurolite composition of the JWGC metapelites

	Kyanite		Chloritoid				Staurolite		
	K-10	K-10A	K-11	K-11	K-10A	K-10A	K-11	K-11	K-21
	1	2	1	2	3	4	1	2	3
SiO_2	36.58	36.93	23.84	23.74	23.82	23.97	27.58	27.71	27.48
TiO_2	0.03	0.01	0.02	0.04	0.01	0.17	0.42	0.34	0.54
Al_2O_3	63.44	62.38	40.40	40.27	39.91	40.22	55.89	55.64	53.30
FeO	0.59	0.61	25.12	24.43	24.54	24.83	11.70	11.83	14.12
MnO	0.02	0.00	0.26	0.29	0.00	0.04	0.26	0.19	0.31
MgO	0.00	0.02	2.64	2.36	3.03	3.12	0.98	1.05	1.69
CaO	0.00	0.07	0.00	0.00	0.05	0.01	0.00	0.00	0.00
Na_2O	0.01	0.05	0.00	0.02	0.00	0.00	0.00	0.02	0.03
K_2O	0.00	0.04	0.00	0.00	0.03	0.02	0.01	0.00	0.00
BaO	0.00	0.05	0.00	0.27	0.28	0.01	0.00	0.20	0.00
P_2O_5	0.14	0.00	0.06	0.00	0.14	0.09	0.00	0.00	0.00
ZnO	0.00	0.22	0.00	0.00	0.14	0.00	2.05	2.64	0.56
Total	100.81	100.38	92.34	91.41	91.93	92.47	98.89	99.62	98.04
	Cation per 20 O		Cation per 14 O OH				Cation per 48 O		
Si	3.929	3.992	1.981	1.991	1.987	1.984	7.899	7.918	7.992
Al	8.032	7.947	3.957	3.982	3.925	3.924	18.868	18.741	18.270
Fe^{+2}	0.000	0.000	1.745	1.714	1.712	1.719	2.803	2.827	3.434
Ti	0.002	0.001	0.001	0.003	0.001	0.011	0.090	0.074	0.118
Mg	0.000	0.003	0.327	0.295	0.377	0.385	0.419	0.446	0.734
Mn	0.000	0.000	0.018	0.021	0.000	0.003	0.063	0.046	0.076
Na	0.003	0.011	0.000	0.003	0.000	0.000	0.001	0.012	0.017
Ca	0.000	0.008	0.000	0.000	0.004	0.001	0.000	0.000	0.000
K	0.000	0.005	0.000	0.000	0.003	0.002	0.005	0.000	0.000
Ba	0.000	0.002	0.000	0.009	0.009	0.000	0.000	0.022	0.000
Zn	0.000	0.017	0.000	0.000	0.009	0.000	0.433	0.557	0.120
P	0.013	0.000	0.004	0.000	0.010	0.006	0.000	0.000	0.000
OH			4.000	4.000	4.000	4.000			
Total	12.034	12.042	12.033	12.018	12.037	12.035	30.581	30.644	30.763

Table 6
Chlorite and epidote composition of the JWGC metapelites

	Chlorite					Epidote	
	K-88	K-81	K-85	K-11		K-13	K-89
	1	2	3	4		1	2
SiO_2	24.97	25.37	25.37	23.28		37.31	37.91
Al_2O_3	22.96	22.58	22.58	22.96		27.04	26.23
TiO_2	0.09	0.08	0.08	0.10		0.11	0.19
FeO	19.77	22.27	22.27	28.75		8.10	8.85
MnO	0.07	0.10	0.10	0.09		0.26	0.15
MgO	18.15	16.09	16.09	11.60		0.07	0.00
CaO	0.01	0.02	0.02	0.03		22.21	23.44
Na_2O	0.04	0.00	0.07	0.00		0.04	0.00
K_2O	0.04	0.02	0.02	0.05		0.00	0.02
P_2O_5	0.00	0.14	0.14	0.03		0.11	0.05
Cr_2O_3	0.00	0.00	0.07	0.00		0.00	0.09
BaO	0.00	0.00	0.00	0.00		0.00	0.08
Total	86.10	86.67	86.81	86.89		95.25	97.01
	Cations per 28 O and 16 OH					12.5 O and .5 OH	
Si	5.203	5.246	5.318	5.061	Si	2.973	2.982
Aliv	2.979	2.754	2.682	2.939	Aliv	0.027	0.018
Alvi	2.842	2.863	2.896	2.945	Alvi	2.512	2.413
Ti	0.013	0.029	0.013	0.016	Cr	0.007	0.005
Fe^{+2}	3.446	5.164	3.905	5.229	Fe3	0.540	0.582
Mn	0.012	0.041	0.017	0.017	Mn3	0.000	0.000
Mg	5.637	3.810	3.760	3.760	Mg	0.008	0.000
Ca	0.002	0.004	0.006	0.006	Ti	0.007	0.011
Na	0.015	0.000	0.000	0.000	Mn2	0.018	0.010
K	0.010	0.014	0.014	0.014	Ca	1.896	1.975

investigated garnet schist (K-13, K-81 and K-89) both garnet core as well as rim temperatures have been obtained. Estimation of the *P–T* conditions was also obtained using TWQ program for coexisting garnet, plagioclase, biotite and muscovite in garnet schist (K-13; Fig. 5). A perusal of the data shows following

- There is practically no difference in estimated temperature for all the formulations when 4- or 6-kbar pressure is considered.
- Within each formulation the range of temperature varies generally within 50 °C (generally the reported error range). This is considering core as well as rim temperatures.
- The estimated core temperatures vary between 500 and 560 °C for K-13 and K-81 while the rim temperatures vary between 492 and 575 °C. The variation between core and rim temperatures is ~25 °C which is within the reported error range of these formulations.
- The intersection of three univariant reactions (TWQ software; Fig. 5) is nearly at a point and it gives a temperature of 500 °C at 6 kbar pressure. Thus, crustal depths in the range of 18–20 km is indicated for the regional metamorphism.
- The temperature estimation by garnet-biotite exchange reaction is corroborated by the Ti in biotite geothermometer (Lal, 1991).

5.2. Granite

In context of thermal metamorphism of the enclaves of the calc silicates by the JWGC granite, the temperature of granite magma is of importance and an attempt is made to estimate the magma temperature of the two feldspar one mica type which is the most dominant variant. One sample of the amphibole granite has also been included in these estimations.

Zircon saturation and magma temperature. Zircon is a nearly ubiquitous accessory mineral in the granitic rocks. It has been a subject of considerable study especially by the geochronologists for its immense utility in U–Pb isotope systematics. These studies have shown that zircon can survive crustal melting events as numerous older zircons have been dated in younger magmatic rocks. The other facet of studies on zircon is the experimental work on its saturation systematics (e.g. Watson, 1979). Based on detailed experimental data, Watson and Harrison (1983) have given a model of zircon solubility in form of the following equation

$$\ln D_{Zr}^{Zircon/Melt} = \{-3.80 - [0.85(M-1)]\} + 12900/T$$

where

$\ln D_{Zr}^{Zircon/Melt}$ ratio of Zr in stoichiometric zircon to that in melt

Table 7
Garnet, clinopyroxene and amphibole composition of the Taranda calc silicates

Sample anal no.	Garnet					Clinopyroxene			Amphibole
	Core K-36B 1	Rim K-36B 2	Core K-36C 3	Rim K-36C 4		Rim K-36B 1	Core K-36B 2		K-36A 1
SiO_2	37.60	37.31	37.59	37.59		48.89	49.40		43.13
Al_2O_3	18.85	18.61	20.42	19.30		0.89	0.98		12.44
TiO_2	0.11	0.16	0.00	0.03		0.01	0.03		0.80
FeO	16.48	16.13	18.48	19.20		23.64	23.50		18.15
MnO	1.68	1.30	2.71	1.10		0.61	0.54		0.64
MgO	0.17	0.15	0.00	0.00		3.16	3.32		8.58
CaO	24.90	25.81	20.46	22.00		22.66	22.90		11.68
Na_2O	0.00	0.00	0.00	0.00		0.25	0.32		0.93
K_2O	0.00	0.00	0.00	0.00		0.00	0.00		1.11
Cr_2O_3	0.00	0.00	0.05	0.00		0.00	0.00		0.00
NiO	0.00	0.00				0.04	0.00		0.00
Total	99.79	99.46	99.71	99.27		100.14	101.00		97.48
	Cations per 12 O					Cations per 6 O			23(O)
Si	2.948	2.931	2.967	2.980	Si	1.961	1.960	Si	6.451
Aliv	0.052	0.069	0.033	0.020	Aliv	0.039	0.040	Aliv	1.549
Alvi	1.689	1.654	1.866	1.783	Alvi	0.003	0.006	Alvi	0.644
Cr	0.000	0.000	0.003	0.000	Ti	0.000	0.001	Ti	0.090
Fe^{+3}	0.350	0.396	0.164	0.233	Zr	0.000	0.000	Cr	0.000
Ti	0.006	0.009	0.000	0.002	Fe3	0.054	0.057	Fe3	0.501
Mg	0.020	0.017	0.000	0.000	Zn	0.000	0.000	Mg	1.914
Fe^{+2}	0.731	0.664	1.056	1.040	Cr	0.000	0.000	Fe2	1.770
Mn	0.112	0.087	0.181	0.074	Mg	0.189	0.197	Mn	0.082
Ca	2.092	2.172	1.730	1.868	Ni	0.001	0.000	Zn	0.000
Total	8.000	8.000	8.000	8.000	Fe2	0.738	0.723	NaB	0.129
					Mn	0.021	0.018	NaA	0.141
ANDR	0.181	0.207	0.083	0.118	Ca	0.974	0.974	Ca	1.871
GROS	0.527	0.532	0.500	0.508	Na	0.019	0.025	K	0.212
SPES	0.038	0.029	0.061	0.025	K	0.000	0.000	Ce	0.000
PYRO	0.007	0.006	0.000	0.000	Total	4.000	4.000	F	0.000
ALMA	0.247	0.226	0.356	0.349				OH	2.000
					WO	51.223	51.42	Total	17.353
					EN	9.942	10.388		
					FS	38.835	38.196		

M cation ratio $(Na + K + 2Ca)/(Al \times Si)$
T absolute temperature

Using the above equation temperatures of seven granite samples of JWGC representing all four petrographic variants have been estimated. These along with the calculated ln $D_{Zr}^{Zircon/Melt}$ and M values are given in Table 12. For this calculation ZrO_2 in zircon is taken as 67% (cf. Deer et al., 1997) while the melt Zirconium is taken as the Zr reported by the ICP-AES analysis.

Estimated temperatures are in the rather narrow range of 775–858 °C. Since all these granites are essentially biotite granites, their crystallization temperatures are expected to be in a narrow range. This also suggests that the zircon in these granites is not xenocrystic. Temperature range of >800 °C and absence of xenocrystic zircons is indicative of I-type nature of JWGC granites as S-type granites are generally ~ 700 °C.

Apatite saturation and magma temperature. Similar to zircon, apatite is also a very common accessory mineral of all magmatic rocks. On account of the ability of apatite to incorporate REE and U, it is of importance to understand the relation of its crystallisation and magma genesis as these incorporated elements are often used for petrogenetic interpretations. As interpreted above for zircon, it is of significance to distinguish between xenocrystic and locally crystallised apatite.

Experimental data in felsic melts at temperatures between 850 and 1500 °C involving dissolution of apatite crystals in hydrous, apatite undersaturated melts has been used to derive an expression of the following type

$$\ln D_P^{Apatite/Melt} = [(8400 + ((SiO_2 - 0.5)2.64 \times 104))/T] - [3.1 + (12.4(SiO_2 - 0.5))]$$

where

SiO_2 weight fraction of silica in the melt
$\ln D_P^{Apatite/Melt}$ concentration ratio of P_2O_5 in apatite to that in melt

Table 8
Plagioclase composition of the Taranda calc silicates

	K-36A	K-36A Rare	K-36C Matrix	K-36C Incl.in gr	K-36C Ad. to gr	K-36C Near gr	K-36C Away from gr	K-66
SiO_2	46.40	65.77	57.80	66.55	66.28	61.98	59.39	57.97
Al_2O_3	34.54	19.31	26.34	20.81	21.56	23.75	25.25	26.50
TiO_2	0.05	0.00	0.02	0.00	0.02	0.00	0.00	0.00
FeO	0.10	0.38	0.29	0.35	0.46	0.33	0.29	0.32
MnO	0.05	0.00	0.00	0.01	0.00	0.10	0.00	0.00
MgO	0.00	0.00	0.00	0.11	0.00	0.00	0.00	0.03
CaO	17.58	0.05	8.39	1.55	2.52	5.25	7.16	8.16
Na_2O	1.62	0.16	7.06	11.02	10.65	8.82	7.68	7.24
K_2O	0.02	14.79	0.12	0.11	0.10	0.15	0.17	0.19
Cr_2O_3	0.04	0.00	0.02	0.00	0.05	0.00	0.00	0.41
P_2O_5		0.00	0.01	0.00	0.03	0.00	0.00	0.00
Total	100.40	100.46	100.05	100.51	101.67	100.38	99.94	100.82
	Cations per 8 O							
Si	2.127	2.993	2.591	2.911	2.876	2.745	2.654	2.589
Al	1.867	1.036	1.392	1.073	1.103	1.240	1.330	1.395
Fe^{+3}	0.004	0.014	0.011	0.013	0.017	0.012	0.011	0.012
Ti	0.002	0.000	0.001	0.000	0.001	0.000	0.000	0.000
Mg	0.000	0.000	0.000	0.007	0.000	0.000	0.000	0.002
Na	0.144	0.014	0.613	0.935	0.896	0.757	0.665	0.627
Ca	0.863	0.002	0.403	0.073	0.117	0.249	0.343	0.390
K	0.001	0.859	0.007	0.006	0.005	0.008	0.010	0.011
Total	5.008	4.918	5.017	5.017	5.014	5.012	5.013	5.026
OR	0.10	98.10	0.70	0.60	0.50	0.80	1.00	1.00
AB	14.30	1.60	60.00	92.20	88.00	74.60	65.40	61.00
AN	85.60	0.30	39.30	7.20	11.50	24.60	33.60	38.00

Ad., adjacent; incl., inclusion; gr, garnet.

Table 9
Epidote and chlorite composition of the Taranda calc silicate

Sample	Epidote					Chlorite
	K-36B 1	K-36C 2	K-37 3	K-37 4		K-36A 1
SiO_2	38.18	37.89	37.1	38.95		26.6
Al_2O_3	25.48	25.53	17.15	19.82		20.24
TiO_2	0.22	0.09	1.36	0.09		0.02
FeO	10.18	9.12	3.01	4.46		26.24
MnO	0.15	0.17	0.07	0		0.32
MgO	0	0	1.91	0.12		14.86
CaO	23.66	23.65	35.84	35.32		0.1
Na_2O	0.01	0.05	0.22	0		0
K_2O	0.01	0.01	0	0.02		0.05
P_2O_5		0.08	0	0		0
Cr_2O_3	0	0	0.01	0		0.14
Total	97.89	96.59	96.67	98.78		88.57
	Cation per 12.5 O and 0.5 OH					28 O,16OH
Si	2.983	2.998	3.054	3.107	Si	5.578
Aliv	0.017	0.002	0	0	Aliv	2.422
Alvi	2.329	2.379	1.673	1.864	Alvi	2.581
Cr	0	0	0	0	Ti	0.003
Fe^{+3}	0.665	0.604	0.208	0.298	Fe2	4.601
Mn^{+3}	0	0	0	0	Mn	0.057
Mg	0	0	0.234	0.015	Mg	4.645
Ti	0.013	0.005	0.084	0.005	Ca	0.023
Mn^{+2}	0.01	0.011	0.005	0	Na	0
Ca	1.98	2.005	3.161	3.019	K	0.013

Table 10
Allanite, biotite and sphene composition of the Taranda calc silicate

	Allanite	Biotite		Sphene
	K-36A 1	K-36A 2		K-36A 3
SiO_2	34.73	36.77		30.48
Al_2O_3	22.5	15.78		3.5
TiO_2	0.3	1.91		34.73
FeO	8.29	19.69		0.7
MnO	0.17	0.23		0.01
MgO	0.41	11.27		0.02
CaO	17.47	0.01		27.95
Na_2O	0.01	0.8		0
K_2O	0	8.43		0.14
Cr_2O_3	0.04	0.01		0
NiO	0.02	0.14		0
Total	83.94	94.32		97.52
		22 (O) 4 (OH)		20 (O, OH)
Si		5.648	Si	1
Aliv		2.352	Al	0.136
Alvi		0.503	Fe3	0.007
Cr		0	Mg	0.001
Ti		0.221	Ti	0.857
Fe^{+2}		2.53	Fe2	0.012
Zn		0	Na	0
Mn		0.03	Ca	0.982
Mg		2.581	K	0.006
Ca		0.001	OH	0.147
Ba		0	Total	3.148
Na		0.022		
K		1.652		
OH		4		
Total		19.541		

Inverse of absolute temperatures ($(1/K)\times 10^4$) for various SiO_2 compositions has been plotted against experimentally arrived ln $D_P^{Apatite/Melt}$ (Watson and Capobianco, 1981). Sample numbers K-28 and K-47 give a magma temperature of ~870 °C which is in consonance with that obtained from the zircon saturation equation. However, for K-48, a very high temperature of ~1130 °C is indicated. In this rock the P_2O_5 content is much higher (0.84 wt %) than that reported for average range of granite rocks (0.01–0.12%; White and Chappell, 1977; Bateman and Chappell, 1979). This is suggestive of carrying of unmelted apatite from the source region while in case of the other two rocks the melt left their source with only the amount of P_2O_5 dissolved in the melt at saturation.

5.3. Calc silicates

The calc silicates preserves contact metamorphic assemblages. In small domains equilibrium conditions can be assumed as indicated by the smooth grain boundary contacts between garnet and clinopyroxene. Thus, garnet-clinopyroxene geothermometer (Fe–Mg exchange) can be employed for the Taranda Calc silicates. For pressure calculation, garnet-clinopyroxene-plagioclase-quartz association is utilized. The results are given in Table 13. Formulations of Krogh (1988); Sengupta et al. (1989) give temperatures between 633 and 700 °C and have very low pressure dependence. A pressure of over 6 kbar (Table 13) is indicated by the Newton and Perkins (1982) formulation. The temperature estimates for the Taranda calc silicates are 100–150 °C higher than those for the metapelites.

6. Metamorphism

In the JWGC, both, regional as well as thermal metamorphic imprints are apparent. The west to east sequence of kyanite, chloritoid, St-1, garnet and St-2 schists in metapelites can be used to decipher a sequence of metamorphic reactions. Muscovite + aluminosilicate

Table 11
Garnet–biotite and Ti in biotite geothermometry of the JWGC metapelites

Garnet-Biotite	K-13	K-13	K-13	K-13	K-81	K-81	K-81	K-81	K-89	K-89	K-89	K-89
	4 Kb C	4 Kb R	6 Kb C	6 Kb R	4 Kb C	6 Kb C	4 Kb R	6 Kb R	4 Kb C	4 Kb R	6 Kb C	6 Kb R
Ferry and Spear 1978	528	553	535	561	529	506	499	536	495	473	502	480
Dasgupta et al., 1991	520	508	529	517	518	492	484	527	495	467	504	475
Bhattacharya et al., 1992	553(534)	573(571)	554(536)	574(573)	560(532)	542(517)	541(515)	561(534)	562(566)	545(551)	563(568)	546(552)

Ti in biotite	K-13	K-81	8.85	K-88	8-75A	8–21	K-89
Temperature °C	562	618	524	554	591	565	544

For Bhattacharya et al. (1992) number in brackets indicate use of garnet solution model of Ganguly and Saxena (1984); C-core; R-Rim.

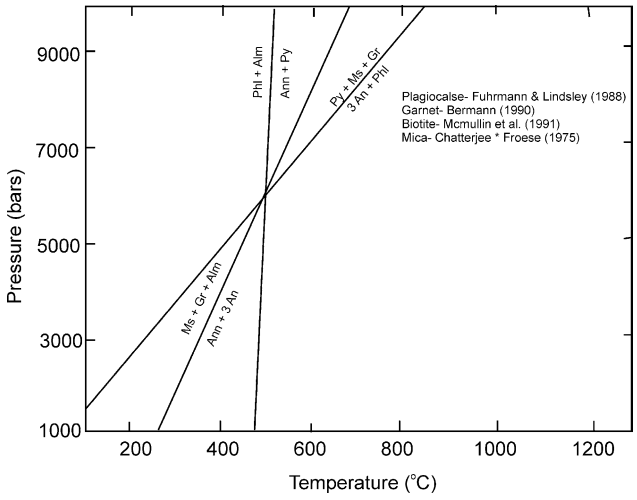

5. TWQ plot of garnet schist (K-13). Three univariant reactions are shown and these intersect at ~500 °C and 6 kbar. (Mineral Abbreviations: Phl-Phlogopite, Alm-Almandine, Ann-Annite, Py-Pyrope, Ms-Muscovite, Gr-Grossular, An-Anorthite): Fuhrmann and Lindsley (1988); Bermann (1990); McMullin et al. (1991); Chatterjee and Froese (1975).

(kyanite) in presence of quartz is the lowest grade assemblage present at the westernmost margin of the JWGC. Chloritoid + kyanite assemblage succeeds the lowest grade rock. The presence of kyanite at low grade typifies the western bed of the JWGC metapelite as high Al-type (Spear, 1993). The chloritoid producing reaction generally involves chlorite and an aluminosilicate e.g.,

Fe Chlorite + Al-silicate/pyrophyllite

= chloritoid + quartz + H_2O

The reaction marks beginning of the greenschist facies. It has been demonstrated that the chloritoid forms in restricted bulk compositions (more alumina than the total mafic oxides, excess of alumina over alkalies and CaO after calculating micas, paragonite or albite and margarite or epidote, more FeO + MnO than MgO and more FeO + MnO than Fe_2O_3, Halferdahl, 1961; Hoschek, 1967). In the JWGC metapelites, chloritoid bearing assemblage do not contain plagioclase or K feldspar indicating these to be low in alkali as well as in CaO while being rich in alumina locally as borne out by the presence of kyanite.

Staurolite of St-1 zone occurs with chloritoid + chlorite. Kyanite generally disappears in St-1 though rare grains are occasionally observed. Staurolite can form from one of the following reactions (Albee, 1972; Fox, 1975);

Chloritoid + Kyanite

= staurolite + chlorite + quartz + H_2O

Chloritoid + kyanite = staurolite + quartz + H_2O

Chloritoid + kyanite

= staurolite + biotite + quartz + H_2O

It is of particular interest to note that the various reactions proposed to explain the chloritoid to staurolite transformation might be true in rocks of particular bulk compositions. Also, in a particular bulk composition, various reactions may be correct under different physical conditions. Spear (1993) has depicted the above reactions in AFM projection (Fig. 10-6 of Spear). In an area, those reactions, which change the largest area of the diagram, thus affecting the largest bulk composition, will be commonly observed in field. In the JWGC metapelites, staurolite (of St-1 zone) occurs both with chlorite as well as without it. At this grade staurolite is restricted to the very Fe-rich bulk compositions and, thus, the bulk of westernmost bed of the JWGC metapelite is of high-Al and high Fe composition. Moreover, biotite is nearly absent. In local domains, therefore, the reactions are controlled by minor variations in bulk composition. The JWGC metapelites depict two broad compositions i.e. the westernmost bed in which plagioclase is absent (thus low CaO + Na_2O) and the schist with plagioclase towards east and closer to the JWGC granite.

In the Lukmanier Pass, Switzerland, Fox (1975), described four mineralogical zones bearing following assemblages;

Zone 1—chloritoid–kyanite–chlorite
Zone 2—staurolite–chloritoid–chlorite–kyanite
Zone 3—biotite–staurolite–chloritoid–chlorite–kyanite
Zone 4—biotite–staurolite–garnet–chlorite–kyanite

The zone boundaries were interpreted to be defined by the following univariant equilibria

Chloritoid + kyanite

= staurolite + chlorite + quarts + H_2O

Table 12
12 Zircon saturation temperature of the JWGC granite

	K-28	K-35	K-48	K-25	K-55	K-36	K-47
M	0.813	0.857	0.875	0.0753	0.925	0.872	1.050
Ln $D_{zr}^{Zircon/Melt}$	8.66	7.81	8.21	8.52	8.56	7.71	7.27
Temperature (°C)	775	850	811	792	827	858	792

Table 13
Garnet–clinopyroxene geothermometry and garnet–clinopyroxene–plagioclase–geobarometry in the Taranda calc silicate

Assumed pressure (kbar)	Geothermometry (°C)		Geobarometry (kbar)
	Krogh (1988)	Sengupta et al. (1989)	Newton and Perkins (1982)
6	706	640	
4	701	634	
Assumed temperature (°C)			
700			7.67
600			6.86

Chloritoid + chlorite + muscovite

= staurolite + biotite + quartz + H_2O

Chloritoid + muscovite + quartz

= staurolite + garnet + biotite + H_2O

The description of Zones 1 and 2 (Fox, 1975) are quite similar to those of the westernmost bed of the JWGC metapelite including the lack of disappearance of any mineral from Zones 1 to 2 and the sporadic occurrence of kyanite in Zone 2. However, Zones 3 and 4 of the Lukmanier area are not observed in the JWGC metapelites. Interestingly, the detailed mineralogy of these four zones (Table 1; Fox, 1975) shows another similarity with the presently studied metapelites in the presence of plagioclase in Zones 3 and 4 akin to the matrix of garnet schist and staurolite schist (St-2). The departures, in the metapelites of the JWGC, in rocks corresponding to the Zones 3 and 4 of the Lukmanier area is, therefore, critical to the understanding of evolution of mineral assemblages in these metapelites.

Garnet schist occurs in between St-1 and St-2 and contains biotite, chlorite, muscovite, plagioclase, quartz and ilmenite with rare epidote. No garnet-staurolite association in a thin section could be found. The Mg/Fe ratios of garnets have been used as an indicator of change of grade from greenschist to epidote-amphibolite facies with the average Mg/Fe for lower grade to be 0.057 and for higher grade to be 0.137 (Kamineni, 1976). This ratio varies from 0.089 to 0.124 for the garnets of JWGC metapelites reflecting the transitional nature of the conditions of their formation. In view of these, the first appearance of garnet is likely to be through following reaction;

Fe-chloritoid + annite = almandine + muscovite + H_2O

This marks the lower stability of almandine + muscovite assemblage and first appearance of garnet (garnet isograd) but this reaction is restricted to very high Fe/Mg bulk which is the special case of the JWGC metapelites.

For evaluating the regional metamorphism of the JWGC metapelites a part of the *P–T* grid of KFMASH system of Spear and Cheyney (1989) is shown in Fig. 6. The reactions inferred are shown as bold univariant lines and the reactants and products are labelled. Regional metamorphism appears to be more or less at static pressure equivalent to the crustal depths of ~18–20 km. Intersection of three univariant reactions (Fig. 5) defines the metamorphic conditions for the regional metamorphism as ~500 °C at 6-kbar pressure (unfilled rectangle in Fig. 6) thereby resulting in low to medium grade assemblages. In the calc silicates the resultant assemblage included epidote as the main mafic mineral. In the high-Al metapelites, kyanite was one of the earliest minerals to form at pressure of ~6 kbar. The entire metamorphism appears to have been within the kyanite stability field. For comparison the range of data of the Himalayan metamorphism is shown as the grey shaded area which represents geothermobarometric data of metapelites, amphibolites and granites (data from Searle et al., 1992) and shows the spread of *P–T* estimates. Unfilled square in Fig. 6, just outside the grey shaded area, depicts metamorphic conditions inferred for the garnet schist which is the peak regional metamorphic assemblage of the JWGC metapelite.

6.1. Thermal metamorphism

The Taranda calc silicate sequence (~35 m thick) is located within the JWGC granite. Several beds of the granite are also present within this sequence. Thus, complex thermal metamorphic zonation is expected. There are significant mineralogical differences within the calc silicates with garnet being absent in Zone A, it being a major mineral in Zone B and a minor constituent in Zone C. Plagioclase in Zone A is Ca rich (An_{86}) where it occurs with K feldspar, biotite and clinopyroxene. Following reactions are likely for this assemblage;

Biotite + 3 calcite + 6 quartz

= 3 clinopyroxene + K feldspar + H_2O + 3 CO_2

Hornblende + 3 calcite + 4 quartz

= 3 clinopyroxene + 2 anorthite + 3 CO_2 + H_2O

Clinopyroxene at Taranda is Fe rich in all the three zones while garnet shows variation in composition in Zones B and C (Zone B-$gros_{53}andr_{21}alma_{23}$ and Zone C-$gros_{50}andr_{8}$-$alma_{36}$). It has been shown in garnet produced synthetically (Liou, 1974) that at higher f_{O2} values (higher than Ni-NiO buffer) andradite-grossular are common while with decreasing O_2 fugacity a shift to almandine-grossular-andradite

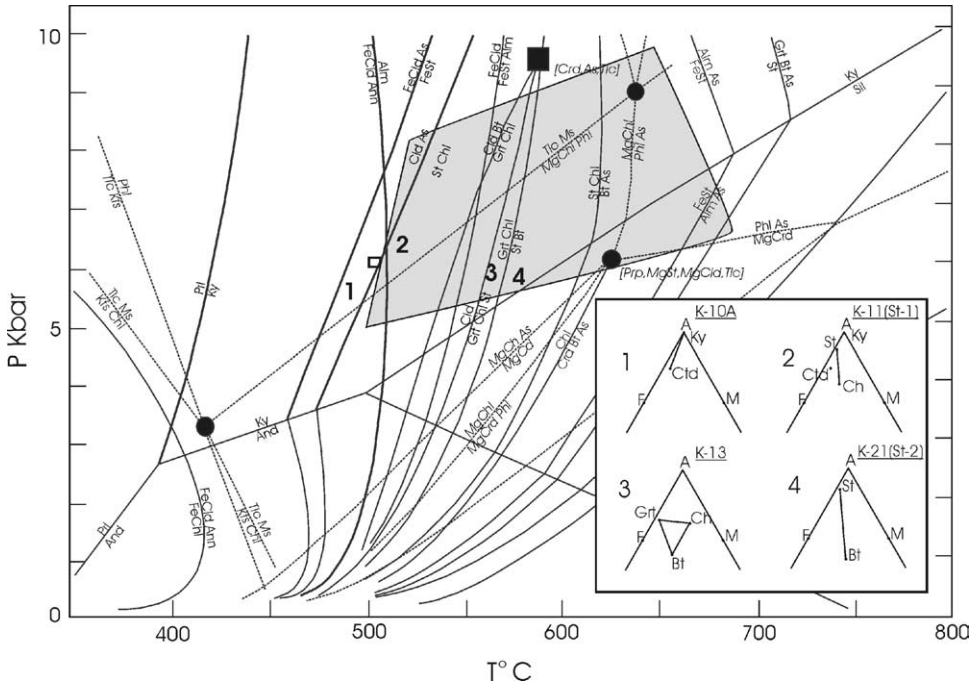

Fig. 6. A part of the *P–T* grid in KFMASH system (From Spear and Cheyney, 1989). Metamorphic reactions relevant to the JWGC metapelites are shown as bold univariant curves. Thompson's AFM projections for these metapelites are given in the inset. The aluminosilicate triple point is after Holdaway (1971). Grey shaded area shows the representative thermobarometric data obtained for the Himalayan metamorphism from metapelites, amphibolites and granites (data from Searle et al., 1992). Unfilled rectangle represents the metamorphic conditions obtained by the intersection of reactions using TWQ programme for the JWGC metapelites.

occurs. As is evident from the variation in garnet composition in Zones B and C it may be inferred that significant f_{O2} variation occurred in distances of the order of few meters during garnet crystallization. Diopside-hedenbergite has been reported from skarns at its junction to the granite-granodiorite batholith (Morgan, 1975) where more diopside rich variant occur with andradite and the more iron rich pyroxene is associated with grossular. The later association is similar to the assemblage in the Taranda calc silicate.

Rarely garnets are developed in Zone C (Fig. 4c). This garnet is solid solution of andradite, grossularite, almandine and spessertine with pyrope being nearly absent ($andr_{8–12}$ $gros_{50–51}$ $alm_{35–36}$ $spess_{3–6}$). The garnet rim is richer in Ca and to a lesser extent in Fe (Table 7) in comparison to the core. Garnet has inclusions of epidote, plagioclase, quartz and calcite and indicates that it formed from epidote in presence of quartz from reactions similar as below.

$$6\ \text{zoisite} = 6\ \text{anorthite} + 2\ \text{grossularite} + \text{corundum} + H_2O$$

$$4\ \text{zoisite} + \text{quartz} = \text{grossularite} + 5\ \text{anorthite} + 2\ H_2O$$

The stability of zoisite and grossularite is dependent upon twin factors of X_{CO2} and presence of quartz (Storre, 1970; Nitsch, 1971). In the absence of quartz grossularite can occur at quite high temperatures (e.g. 875 °C at 2 kbar; Boettcher, 1970) while in presence of quartz it reacts to form wollastonite after 600 °C as is common in contact metamorphic aureoles. In the Taranda calc silicates, wollastonite has not been recorded and quartz is present and thus the temperatures of crystallization of these minerals are inferred to be not more than 600 °C.

Composition of epidote in matrix as well as inclusion in garnet is quite similar (Table 9). However, this is not the case with plagioclase. The plagioclase inclusion is albitic (An_7). The matrix plagioclase immediately adjacent to the rim of garnet is also quite sodic (An_{11}). The anorthite content increases to An_{25} at a distance of ~20 μm from the garnet rim (Fig. 4d) and further 20 μm away it is even more calcic (An_{34}). Steep zoning profile of plagioclase adjacent to the garnet is suggestive of influence of steep and short lived thermal gradient corroborating other textural and mineralogical evidence of thermal metamorphic growth (skarn) in the Taranda Zone. Also, epidote inclusions inside the garnet (illustrating epidote to garnet transformation) imply pre-existing low-grade metamorphic nature of calc silicates in this zone prior to the proximal emplacement of the JWGC granites. Mineral zonation (e.g. amphibole–clinopyroxene and biotite in Zone A and clinopyroxene–epidote and plagioclase in Zone C) has been described earlier. The Taranda calc silicate zone is similar to Crestmore locality in California where lenticular masses of limestone engulfed in quartz–diorite magma were thermally metamorphosed to marble and subsequently developed contact metamorphic assemblages including those containing grossular, diopside and wollastonite in zones up to 15 m wide following

metasomatic alterations as a result of the intrusion of a quartz–monzonite porphyry (Burnham, 1959). In another comparative setting from Scotland where weakly metamorphosed limestone with high Ca/Mg and siliceous dolomite interbedded with pelite and quartzite has been affected by the thermal metamorphism caused by an igneous suite made up of monzodiorite, quartz–diorite and granite (Ballachulish igneous complex). Diopside forms both in limestone as well in siliceous dolomite (Masch and Heuss-Abbichler, 1991). Seven isograds were mapped in this work with the formation of periclase defining the highest grade. The comparatively more varied mineralogy of the Taranda calc silicate probably is a result of a combination of several factors such as relatively higher grade of metamorphism of the protolith, impure nature of carbonate rocks and a stronger role of aqueous fluids as depicted by domainal development of mineral assemblages parallel to contact with the granite, epidote and plagioclase as inclusion minerals in the garnet and local variations in the f_{O2} inferred by the change in garnet compositions.

Contact effect of the JWGC granite is reflected in the assemblage of staurolite schist of St-2. East of garnet schist this thin schist unit occurs associated with biotite, quartz and plagioclase with minimal amount of muscovite. Hoschek (1969) has experimentally investigated the following reaction;

Chlorite + muscovite

= staurolite + biotite + quartz + vapour

The phase boundary (moderately steep, positive slope) for the above reaction is given by the conditions 565 ± 15 °C at 7 kb and 540 °C at 4 kb. This run was determined both on plagioclase bearing as well as plagioclase absent assemblages. This assemblage occurs in a very narrow zone adjacent to the JWGC granite and represents the highest temperature assemblage in the area. Spatial position, localised occurrence and mineral assemblage distinct from St-1 indicate the likelihood of St-2 assemblage a contact effect of the JWGC granite.

Thus, as is clear from above, within a narrow ($\sim$35 m) width of Taranda calc silicates (composed of Zones A, B and C) an intra as well as inter zone heterogeneity of assemblage is present with one of the zone lacking garnet (Zone A). Plagioclase composition is also highly variable from zone to zone. The mineralogical variations are accompanied by the textural variations. These features are definitive indication of thermal metamorphism associated with metasomatism and, therefore, skarn nature of the Taranda Calc Silicate Zone.

7. Conclusions

The JWGC metapelites preserve imprints of low to medium grade metamorphism. The calc silicates were also similarly transformed. The JWGC metapelites host the JWGC granite within which the Taranda calc silicate enclave is present. This enclave is made up of three zones. Magma temperature of the JWGC granite by zircon and apatite saturation is indicated to be over 800 °C. Thermal and metasomatic imprint of the JWGC granite is seen in the Taranda calc silicate in the variation in mineralogy of the three zones as well in the textures developed. Epidote inclusion is present within garnet in these rocks as a relict low-grade regional metamorphic mineral equivalent to those of the JWGC metapelite. Staurolite + biotite assemblage (St-2) is possibly on account of thermal metamorphic imprint of the JWGC granite as it occurs in juxtaposition to the granite.

Since the age of the JWGC granite is well constrained at $\sim$1.8 Ga, its contact effect on the metapelite and calc silicate describe the preservation of palaeoproterozoic thermal metamorphic overprinting over pre-existing low grade regional metamorphic assemblages in this segment of Lesser Himalayas.

Acknowledgements

The Director General, Geological Survey of India is thankfully acknowledged for facilitating participation in 17th Himalayan Karakoram Tibet Workshop, Gangtok, Sikkim and for permitting the publication of this paper. Shri U.K. Bassi, Dy Director General and Shri J.K. Bhalla, Director, EPMA Laboratory provided all the help and encouragement. Sonalika Joshi, Assistant Geologist assisted in the microprobe analysis. D.K. Bhattacharya helped in preparation of the drawings. Two anonymous reviewers led to the improvement of the presentation. Critical and incisive comments of Professor P.K. Verma, Department of Geology, University of Delhi, allowed greater focus in the organization of the manuscript.

References

Albee, A.L., 1972. Metamorphism of pelitic schists: reaction relations of chloritoid and staurolite. Bulletin Geological Society of America 83, 3249–3268.

Bateman, P.C., Chappell, B.W., 1979. Crystallization, fractionation and solidification of the Tuolumne intrusive series, Yosemite National Park, California. Bulletin Geological Society of America 90, 465–482.

Berman, R.G., 1990. Mixing properties of Ca–Mg–Fe–Mn garnets. American Mineralogist 75, 328–344.

Berthelsen, A., 1951. A geological section through the Himalayas. Medd. Donsk. Geol. Foresing. 12, 102–104.

Bhanot, V.B., Kwatra, A.K., Singh, V., Pandey, B.K., 1978. Rb/Sr whole rock age for the Chail Series of Northwestern Himalaya, Himachal Pradesh. Journal Geological Society of India 19, 224–225.

Bhargava, O.N., 1982. The tectonic windows of the Lesser Himalaya. Himalayan Geology 10, 135–155.

Bhargava, O.N., Kedar, N., Dass, A.S., 1972. A note on the Rampur window, district Mahasu. Journal Geological Society of India 13, 277–280.

Bhattacharya, A.K., Mohanty, L., Maji, A., Sen, S.K., Raith, M., 1992. Non-ideal mixing in the phlogopite-annite binary: constraints from experimental data on Mg–Fe partitioning and a reformulation of the biotite–garnet geothermometer. Contribution to Mineralogy and Petrology 111, 87–93.

Boettcher, A.L., 1970. The system CaO–Al2O3–SiO2–H2O at high temperatures and pressures. Journal of Petrology 11, 337–339.

Burnham, C.W., 1959. Contact metamorphism of magnesian limestone at Crestmore, California. Bulletin Geological Society of America 70, 879–920.

Chatterjee, N.D., Froese, E.F., 1975. A thermodynamic study of the pseudobinary join muscovite–paragonite in the system KAlSi3O8–NaAlSi3O8–Al2O3–SiO2–H2O. American Mineralogist 60, 985–993.

Dasgupta, S., Sengupta, P., Fukuoka, M., Bhattacharya, P.K., 1991. Mafic granulites from the Eastern Ghats, India: further evidence for extremely high temperature crustal metamorphism. Journal of Geology 99, 124–133.

Deer, W.A., Howie, R.A., Zussman, J., 1997. Rock Forming Minerals, vol. 1A, Orthosilicates. The Geological Society of London, Oxford p. 919.

Ferry, J.M., Spear, F.S., 1978. Experimental calibration of the partitioning of Fe and Mg between biotite and garnet. Contribution to Mineralogy and Petrology 66, 113–117.

Fox, J.S., 1975. Three-dimensional isograds from the Lukmanier Pass, Switzerland and their tectonic significance. Geological Magazine 112, 547–626.

Frank, W., Thoni, M., Purtscheller, F., 1977. Geology and petrography of Kulu-south Lahul area. in: Himalayas, Science de la Terre, CNRS, Paris, 268, pp. 147–172.

Fuhrman, M.L., Lindsley, D.H., 1988. Ternary-feldspar modelling and thermometry. American Mineralogist 73, 201–216.

Granguly, J., and Saxena, S.K., 1984. Mixing properties of aluminosilicate gamets: constraints from natural and experimental data and application to geothermobaometry. American Mineralogist. 69, 81–97

Gansser, A., 1964. Geology of the Himalayas. Interscience Publishers, London p. 289.

Halferdahl, L.B., 1961. Chloritoid: its composition, X-ray and optical properties, stability and occurrence. Journal of Petrology 2, 49–135.

Holdaway, M.J., 1971. Stability of andalusite and the aluminium silicate phase diagram. Americal Journal of Science 271, 97–131.

Hoschek, G., 1967. Untersuchungen zum stabilitat von chloritoid und staurolite. Contribution to Mineralogy and Petrology 14, 123–162.

Hoschek, G., 1969. The stability of staurolite and chloritoid and their significance in the metamorphism of pelitic rocks. Contribution to Mineralogy and Petrology 22, 208–232.

Jhingran, A.G., Kohli, G, Shukla, B.N., 1952. Geological notes on the traverse to the spiti valley (Punjab) jointly with the third Royal Damish Expedition to central Asia 1950, Geological Survey of India, unpublished report.

Kamineni, D.C., 1976. Coexisting garnet and chlorite in crystalline rocks. neues Jahrbuch Fur Mineralogica monatshefte 1976;, 174–185.

Krogh, E.J., 1988. The garnet-clinopyroxene Fe–Mg geothermometer-a reinterpretation of existing experimental data. Contribution to Mineralogy and Petrology 99, 44–48.

Kwatra, S.K., Bhanot, V.B., Kakkar, R.K., Kamsal, A.K., 1986. Rb–Sr radiomatic age of Wangtu Genissic Complex, Kinnaur district, H.P.. Bullettin, Indian Geological Association 19 (2).

Lal, R.K., 1991. Empirical calibrations of the Ti contents of Biotite and Muscovite for geothermobarometry and their application to low and high grade metamorphic rocks, Third Indo-Soviet Symposium on Experimental Mineralogy and Petrology, New Delhi 1991. 18p..

Leake, B.E., Woolley, A.R., Birch, W.D., Gilbert, M.C., Grice, J.D., Hawthrone, F.C., Kato, A., Kisch, J.H., Krivovichev, V.G., Linthout, K., Laird, J., Mandarino, J., Maresh, W.V., Nickel, E.H., Schumacher, J.C., Stephenson, N.C.N., Whittaker, E.J.W., Youzib, G., 1997. Nomenclature of amphiboles: report of the subcommittee on amphiboles of the International Mineralogical Association Commission on new minerals and mineral names. Mineralogical Migazine 61, 295–321.

LeFort, P., Debon, F., Sonet, J., 1983. The Lower Palaeozoic 'Lesser Himalayan' granitic belt: emphasis on Simcher pluton of Central Nepal, in: Shams, F.A. (Ed.), Granites of Himalayas, Karakoram and Hindu Kush. Punjab University, Lahore, Pakisthan, pp. 235–255.

Liou, J.G., 1974. Stability relations of andradite–quartz in the system Ca–Fe–Si–O–H. American Mineralogist 59, 1016–1025.

Masch, L., Heuss-Abbichler, S., 1991. Decarbonation reactions in siliceous dolomites and impure limestones, in: Voll, G., Topel, J., Pattison, D.R.M., Seifert, F. (Eds.), Equilibrium and Kinetics in Contact Metamorphism: The Ballachulish Igneous Complex and its Aureole. Springer, Berlin.

McMullin, D., Berman, R.G., Greenwood, H.J., 1991. Calibration of the SGAM thermobarometer for pelitic rocks using data from phase equilibrium experiments and natural assemblages. Canadian Mineralogist 29.

Miller, C., Klotzli, U., Frank, W., Thoni, M., Grasemann, B., 2000. Proterozoic crustal evolution in the NW Himalayan (India) as recorded by circa 1.80 Ga mafic and 1.84 Ga granitic magmatism. Precambrian Research 103, 191–206.

Morgan, B.A., 1975. Mineralogy and origin of skarns in the Mount Morrison pendant, Sierra Nevada, California. American Journal of Science 275, 119–142.

Newton, R.C., Perkins, D., 1982. Thermodynamic calibration of geobarometers based on assemblages garnet-plagioclase-orthopyroxene (clinopyroxene)-quartz. American Mineralogist 67, 203–222.

Nitsch, K.H., 1971. Die niedrig Temperaturgrenze des Anorthit-Stabilitatfeldes. Fortshritte der Mineralogie, 49, Beiheft 1, 71-73

Pant, N.C., Kumar, R., Kundu, A., Dorka, B.S., Prasher, S., 2000. Petrology, phase chemistry and its bearing on tin-tungsten mineralisation in Jeori-Wangtu Gneissic complex, Kinnaur District, H.P., (Extended Abstract). Records Geological Survey of India 133 (pt. 8), 91–93.

Parrish, R.R., Hodges, K.V., 1996. Isotopic constraints on the age and provenance of the Lesser and Greater Himalayan sequences, Nepalese Himalaya. Bulletin Geological Society of America 108, 904–911.

Pognante, U., Lombardo, B., 1989. Metamorphic evolution of the High Himalayan Crystallines in SE Zanskar, India. Journal of Metamorphic Geology 7, 9–17.

Rameshwar, R.D., Sharma, K.K., Gopalan, K., 1995. Granitoid rocks of Wangtu Gneissic Complex, Himachal Pradesh: an example of insitu fractional crystallization and volatile action. Journal Geological society of India 46, 5–14.

Searle, M.P., 1999. Emplacement of Himalayan leucogranites by magma injection along giant sill complexes: examples from Cho Oyu, Gyachung Kang and Everest leucogranites (Nepal Himalaya). Journal of Asian Earth Science 17, 773–783.

Searle, M.P., Waters, D.J., Rex, D.C., Wilson, R.N., 1992. Pressure, temperature and time constraints on Himalayan metamorphism from eastern Kashmir and western Zanskar. Journal Geological Society London 149, 753–773.

Sengupta, P., Dasgupta, S., Bhattacharya, P.K., Hariya, Y., 1989. Mixing behavior in quaternary garnet solid solution and an extended Ellis and Green garnet-clinopyroxene geothermometer. Contribution to Mineralogy and petrology 103, 223–227.

Sharma, R., Misra, D.K., 1998. Evolution and resetting of the fluids in Manikaran Quartzite, Himachal Pradesh: application to burial and recrystallization. Journal Geological Society of India 51, 785–792.

Singh, S., Clasesson, S., Jain, A.K., Sjoberg, H., Gee, D.G., Manikavasagam, R.M., Andreasson, P.G., 1994. Geochemistry of the Proterozoic peraluminous granitoids from the Higher Himalayan Crystalline (HHC) and Jutogh Nappe, NW Himalaya, Himachal Pradesh, India. Journal Nepal Geological Society 10, 125.

Spear, F.S., 1993. Metamorphic Phase Equilibria and Pressure–Temperature-Time paths. Monograph Series. Mineralogical Society of America, Washington. 799p.

Spear, F.S., Cheyney, J.T., 1989. A petrogenetic grid for pelitic schists in the system SiO2–Al2O3–FeO–MgO–K2O–H2O. Contribution to Mineralogy and Petrology 101, 149–164.

Storre, B., 1970. Stabilitatsbedingungen Grossular-fuhrender Paragensen im System $CaO–Al_2O_3–SiO_2–CO_2–H_2O$. Contribution to Mineralogy and Petrology 29, 145–162.

Thakur, V.C., 1983. Granites of Western Himalayas and Karakoram, Structural framework, geochronology and tectonics, in: Sharma, F.A. (Ed.), Granites of Himalayas, Karakoram and Hindu Kush. Punjab University, Lahore, Pakistan, pp. 327–339.

Thoni, M., 1977. Geology, structural evolution and metamorphic zoning in the Kulu Valley (Himachal Himalayas, India) with special reference to the reversed metamorphism. Mitteilung der Geselleschaft der Geologie and Bergbaustudenten in Osterreichs 24, 125–187.

Valdiya, K.S., 1980. Geology of Kumaun Lesser Himalaya. Wadia Institute of Himalayan Geology, Dehra Dun, India. 291p.

Verma, P.K., 1989. The Himalayan Metamorphism, in: Daly, J.S., Cliff, R.A., Yardley, B.W.D. (Eds.), Evolution of Metamorphic Belts. Geological Society of London Special Publication 43, pp. 377–383.

Watson, E.B., 1979. Zircon saturation in felsic liquids: experimental data and applications to trace element geochemistry. Contribution to Mineralogy and Petrology 70, 407–419.

Watson, E.B., Capobianco, C.J., 1981. Phosphorous and the rare earth elements in felsic magma: as assessment of the role of apatite. Geochimica et Cosmochimica. Acta 45, 2349–2358.

Watson, E.B., Harrison, T.M., 1983. Zircon saturation revisited: temperature and composition effects in a variety of crustal magma types. Earth and Planetary Science Letters 64, 295–304.

White, A.J., Chappell, B.W., 1977. Ultrametamorphism and granitoid genesis. Tectonophysics 43, 7–22.